

See discussions, stats, and author profiles for this publication at: <https://www.researchgate.net/publication/237095225>

Time-Resolved Spectroscopic Characterization of a Novel Photodecarboxylation Reaction Mediated by Homolysis of a Carbon α -Bond in Flurbiprofen

ARTICLE in THE JOURNAL OF PHYSICAL CHEMISTRY B · JUNE 2013

Impact Factor: 3.3 · DOI: 10.1021/jp403053f · Source: PubMed

CITATIONS

2

READS

50

4 AUTHORS, INCLUDING:



Tao su

Shanghai Institute of Applied Physics

16 PUBLICATIONS 100 CITATIONS

[SEE PROFILE](#)



Nai-Kei Wong

The University of Hong Kong

19 PUBLICATIONS 214 CITATIONS

[SEE PROFILE](#)



David Lee Phillips

The University of Hong Kong

346 PUBLICATIONS 7,056 CITATIONS

[SEE PROFILE](#)

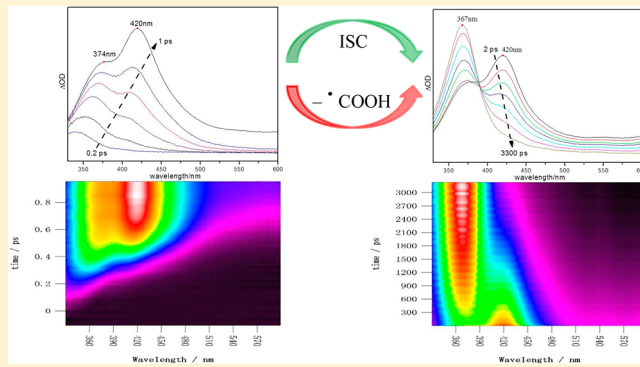
Time-Resolved Spectroscopic Characterization of a Novel Photodecarboxylation Reaction Mediated by Homolysis of a Carbon α -Bond in Flurbiprofen

Tao Su, Jiani Ma, Naikei Wong, and David Lee Phillips*

Department of Chemistry, The University of Hong Kong, Pokfulam Road, Hong Kong, P. R. China

Supporting Information

ABSTRACT: Flurbiprofen (Fp), a nonsteroidal anti-inflammatory drug (NSAID) currently in use for arthritis pain relief and in clinical trials for metastatic prostate cancer, can induce photosensitization and phototoxicity upon exposure to sunlight. The mechanisms responsible for Fp phototoxicity are poorly understood and deserve investigation. In this study, the photodecarboxylation reaction of Fp, which has been assumed to underpin its photoinduced side effects, was explored by femtosecond transient absorption (fs-TA), nanosecond transient absorption (ns-TA), and nanosecond time-resolved resonance Raman (ns-TR³) spectroscopic techniques in pure acetonitrile (MeCN) solvent. Density functional theory (DFT) calculations were also performed to facilitate the assignments of transient species. The resonance Raman and DFT calculation results reveal that the neutral form of Fp was the predominant species present in MeCN. Analysis of the ultraviolet/visible absorption spectrum and results from TD-DFT calculations indicate that the second excited singlet (S_2) can be excited by 266 nm light. Due to its intrinsic instability, S_2 rapidly underwent internal conversion (IC) to decay to the lowest lying excited singlet (S_1), which was observed in the fs-TA spectra at very early delay times. Intriguingly, three distinct pathways for S_1 decay seem to coexist. Specifically, other than fluorescence emission back to the ground state and transformation to the lowest triplet state T_1 through intersystem crossing (ISC), the homolysis of the carbon α -bond decarboxylation reaction proceeded simultaneously to give rise to two radical species, one being carboxyl and another being the residual, denoted as FpR. The coexistence of the triplet Fp (T_1) and FpR species was verified by means of TR³ spectra along with ns-TA spectra. As a consequence of its apparent high reactivity, the FpR intermediate was observed to undergo oxidation under oxygen-saturated conditions to yield another radical species, denoted as FOR, which subsequently underwent intramolecular hydrogen transfer (IHT) and dehydroxylation (DHO) to form a final product, which could react with the carboxyl from the decarboxylation reaction to generate a minor final product. TD-DFT and transient state (TS) calculations for predicting the absorption bands and activation energies of the transient species produced in the photodecarboxylation reaction have provided valuable mechanistic insights for the assignment of the intermediate species observed in the time-resolved spectroscopy experiments reported here. The results of the time-resolved spectroscopy experiments and DFT calculations were used to elucidate the reaction mechanisms and intermediates involved in the photochemistry of Fp.



INTRODUCTION

Flurbiprofen (2-fluoro- α -methyl-4-biphenylacetic acid) is a representative 2-arylpropionic acid that can be used as a nonsteroidal anti-inflammatory drug (NSAID). Flurbiprofen (denoted hereafter as Fp) has been widely prescribed as an anti-inflammatory, antipyretic, and analgesic agent for several therapeutic applications such as pain from rheumatoid arthritis,^{1–4} sunburn^{5,6} and acute gout,⁶ migraine headache,^{7,8} osteoarthritis,^{9–12} soft tissue injuries (tendinitis and bursitis),^{13,14} postoperative ocular inflammation (e.g., excimer laser photorefractive keratectomy),^{12,15–18} vernal keratoconjunctivitis,¹⁹ ocular gingivitis,²⁰ and herpetic stromal keratitis.²¹ Pharmacologically, Fp effects are mediated via inhibition of cyclooxygenase enzymes (COX-1 and COX-2, also referred to as prostaglandin H₂ synthases). These enzymes are responsible

for the conversion of arachidonic acid into prostaglandin H₂, a key intermediate in the biosynthetic pathway of prostaglandins, prostacyclines, and thromboxanes.^{15,17} Additionally, Fp has been exploited as a probe to displace fluorescent cyclooxygenase inhibitors from the active sites, from which emission changes can be analyzed to provide mechanistic insights about the protein–drug interactions between such inhibitors and COX-1/COX-2.^{18,19}

Fp has also been reportedly associated with a variety of adverse side effects like ulcerations, abdominal burning, cramping, nausea, gastritis, drowsiness, and stuffy nose. More

Received: March 28, 2013

Revised: June 4, 2013

Published: June 10, 2013

severe forms of side effects from using Fp are associated with chest pain, confusion, dark urine, depression, weakness, vision or speech changes, vomiting, and yellowing of the skin or eyes.²² In addition, Fp photoproducts generated by exposure to sunlight in the skin appear to impart dramatically toxic effects on cell membranes and lead to a noxious photoallergic contact dermatitis in clinical practices²³ due to Fp's biphenyl structure that confers on the drug a high solubility in lipids. Photosensitivity, phototoxicity, and photoallergic responses are among the most common side effects of NSAIDs, especially for the 2-arylpropionic acid derivatives as a result of the special chiral structure in the side chain. Some of these structures are shown in Figure 1.

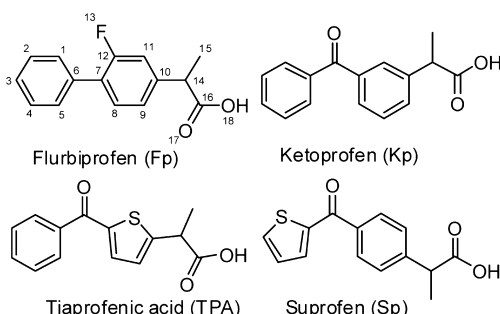


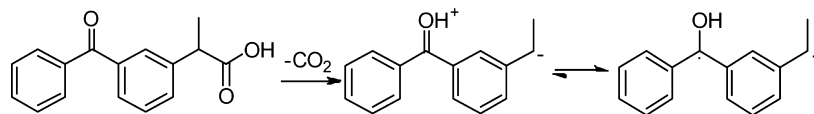
Figure 1. Formulas of four related NSAID compounds: Fp, Kp, TPA, Sp.

With respect to ketoprofen (Kp), suprofen (Sp), and tiaprofenic acid (TPA), a substantial number of studies have been conducted that utilized time-resolved techniques including laser flash photolysis and nanosecond time-resolved resonance Raman (ns-TR³) spectroscopies.^{24–33} These studies led to degradation mechanisms being proposed by several research groups.^{24,26,32} Kp has gained much more attention than other NSAIDs in that it is a derivative of benzophenone (Bp), which is a common photosensitizer in photochemistry with a near-unity conversion from the lowest lying excited singlet S₁ to the lowest lying triplet state T₁. Furthermore, in biological systems, Bp has been extensively used as photochemical probes to identify and map peptide–protein interactions.³⁴ In early studies, the research groups of Wan and Scaiano independently proposed Kp decarboxylation mechanisms in which a radical versus a carbanion can be prone to act as the intermediate that is from decarboxylation based on multiple lines of experimental evidence.^{35–37} Later, Phillips and co-workers directly observed these carbanion and biradical intermediates by femtosecond transient absorption spectra (fs-TA) and TR³, which elucidated the decarboxylation mechanism of Kp by heterolytic cleavage of a carbon–carbon bond (see Scheme 1).^{32,38} With regard to TPA and Sp, decarboxylation mechanisms similar to that of Kp have been put forward by Miranda and co-workers.^{24,39} In contrast, limited investigations^{21,40–42} were directed toward illuminating the detailed photodegradation mechanisms of Fp, due to the

highly complex deactivation routes of the lowest lying excited singlet S₁ involving fluorescence emission back to the ground state, transformation to the lowest lying excited triplet T₁ via intersystem crossing (ISC) with high quantum yields, and a plausible photodecarboxylation reaction. In addition, a unique feature for Fp degradation compared with those of other NSAIDs (Kp, Sp, TPA, etc.) is that Fp photodecarboxylation can proceed in pure acetonitrile (MeCN),⁴⁰ whereas there is no sign of a similar degradation observed for Kp, SP, TPA, etc. in MeCN. Preliminarily, Miranda and co-workers carried out studies of phototoxicity of Fp in vitro and found it to be photolabile and able to generate several photoproducts through a primary photochemical mechanism involving initial cleavage of the C–C bond α to carbonyl group, followed by several secondary processes.⁴⁰ Afterward, they employed steady-state and laser flash photolysis techniques to investigate the photophysical and photochemical properties of Fp in four diverse solutions including MeCN, MeOH, hexane, and phosphate-buffered aqueous solution (PBS) and analyzed the photoproducts formed (mainly four products, see Figure 2). In MeCN, the major species of the photoproducts observed is 1, which accounts for 97% of the total products, while trace amounts of 2 constituting only 3% were also seen.⁴⁰ In PBS solution which is one kind of aqueous solution simulating a biological-like environment, three products could be observed: 1 (23%), 3 (50%), and 4 (27%).⁴⁰ Due to the presence of OH[−] in aqueous solution, the substitution reaction for the fluorine with OH[−] also took place. This and the observation of a new product 3 in the PBS solution indicate that the solvent has an important effect on the photoreaction.⁴⁰ Wu and co-workers also performed characterization experiments for Fp irradiated in methanol and identified four major photoproducts, which they presumed to be derived by esterification and decarboxylation and thus proposed a simple degradation mechanism.⁴¹ To simplify analysis of the reactive intermediates and reaction mechanisms involved in the photochemistry of Fp, we have focused here on the photoreaction mechanism in MeCN solution which mainly produces 97% photoproduct 1 that is also the major product (87%) observed after photoexcitation in CH₃OH and also a significant product (23%) in the PBS solution.⁴⁰ The work here will serve as an initial step to better understand the photochemistry of Fp in solution-phase environments and can be used later to help elucidate the more complex competing reactions that take place in a PBS solution where three significant photoproducts (1 (23%), 3 (50%), and 4 (27%)) are observed compared to mainly 97% photoproduct 1 in the MeCN solution.⁴⁰

Although valuable information has been gained from these previous studies, there remains some crucial unanswered questions; for example: What are the initial photophysical events involved in Fp photodegradation and what is the unambiguous structural basis for the multiplicity and character of the reactive intermediates? Further experimental investigation is required to firmly establish the multiplicity of the reactive intermediate for the photodecarboxylation reaction and unambiguously identify the reactive intermediates themselves.

Scheme 1. Proposed Photodecarboxylation Mechanism of Kp



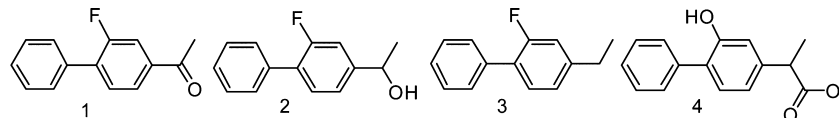


Figure 2. Photoinduced decarboxylated products of Fp in different solutions.

Time-resolved spectroscopy experiments offer several advantages in elucidating the photophysical processes and reactive intermediates involved in photochemical reactions of interest. Vibrational spectroscopic methods like resonance Raman spectroscopy can provide structural and fingerprint information for chemical compounds and intermediates in temporally dynamic systems. In the study reported here, resonance Raman spectroscopy experiments and density functional theory (DFT) calculations were employed to characterize and identify the ground state species of Fp that are photoexcited in MeCN. Furthermore, femtosecond and nanosecond transient absorption spectroscopies were applied to characterize the photophysics and photochemistry of Fp in MeCN to help shed light on the photodecarboxylation pathway and photochemical intermediates. TR³ spectroscopy was also used to identify the intermediates observed in the photodecarboxylation reaction by supplying key structural and fingerprint details. DFT calculations were performed to aid our analysis of the properties and features of the intermediates and transition states associated with the reactions of interest. Collectively, our results provide new mechanistic insights into the intriguingly complex Fp photochemistry by characterizing the photodecarboxylation reactions of this NSAID compound in MeCN.

■ EXPERIMENTAL AND COMPUTATIONAL METHODS

Materials. Flurbiprofen (denoted as Fp) was commercially obtained from Aldrich (with >97% purity) and used as received. The solutions used in the resonance Raman experiments were prepared at a concentration of 1.0 mM. The samples used for ns-TA experiments under oxygen- or nitrogen-saturated conditions were purged with the appropriate gas for about 30 min.

Steady-State UV/Vis Absorption. Steady-state absorption spectra were recorded by a PerkinElmer Lambda 19 UV/vis spectrometer with a 1 cm path length quartz cuvette.

Fs-TA Experiments. Fs-TA measurements were performed with a femtosecond Ti:sapphire regenerative amplifier and an automated data acquisition system. The amplifier was seeded with a 120 fs output from the oscillator laser. The probe pulse was obtained by using approximately 5% of the amplified 800 nm output from the amplifier to generate a white-light continuum (320–800 nm) through a CaF₂ crystal. The maximum extent of the temporal delay was about 3200 ps for the optical stage used in the experiments and the instrument response function was determined to be 150 fs. At each temporal delay, the data were averaged for 2 s. The probe beam was split into two before passing through the sample with one beam traveling through the sample and another passing directly through the reference spectrometer that monitors the fluctuations in the probe beam intensity. Two fiber optics were coupled to a multichannel spectrometer with a CMOS sensor that had a 1.5 nm intrinsic resolution. For the present experiments, the sample solutions were excited by a 267 nm pump beam (the third harmonic of the fundamental 800 nm from the regenerative amplifier). Samples (60 mL solutions)

passed through a 2 mm path length cuvette with a sample concentration of 0.14 mM maintained throughout data acquisition. The data were stored as three-dimensional wavelength-time-absorbance matrices that were exported for use with a fitting software.

Ns-TA Experiments. Nanosecond time-resolved transient absorption (ns-TA) measurements were carried out with a LP920 laser flash spectrometer provided by Edinburgh Instruments Ltd. The probe light source was a 450 W ozone-free Xe arc lamp with 10 Hz to single shot operation in a versatile sample chamber (equipped with integral controller, high-speed pump, probe port shutters, sample holder, and filter holders) which produces a continuous spectrum between 150 and 2600 nm. Measurements of the ns-TA spectra were performed according to the following procedures. Fresh sample solutions were excited by a Q-switched Nd:YAG laser (fourth harmonic line at $\lambda = 266$ nm). The probe light from a pulsed xenon arc lamp passed through various optical elements, samples, and a monochromator before being detected by a fast photomultiplier tube and recorded with a TDS 3012C digital signal analyzer. In the kinetics mode, a photomultiplier detector or InGaAs PIN detector was used and the transient signal was rapidly acquired with a high-resolution oscilloscope. In the spectral mode, an array detector was fitted to the spectrograph exit port to measure a full range of wavelengths simultaneously. About 4 mL solutions were employed in a 10 mm path length cuvette with a sample concentration of 0.086 mM maintained throughout data acquisition.

Ns-TR³ Experiments. The ns-TR³ experiments were done using an experimental apparatus and methods discussed in detail previously,^{43,44} so only a brief description will be given here. The 266 nm pump laser pulse generated from the fourth harmonic of a Nd:YAG nanosecond pulsed laser and a 416 nm probe laser pulse generated from the first Stokes hydrogen Raman shift laser line from the third harmonic were used in the ns-TR³ experiments to detect the transient species arising from the decarboxylation reaction of interest. The energies for the pump and probe pulses were in the range of 2.5–3.5 mJ with a 10 Hz repetition rate. The two Nd:YAG lasers were synchronized electronically by a pulse delay generator to control the time delay of the pump and probe lasers monitored by a fast photodiode and 500 MHz oscilloscope, and the time resolution for the ns-TR³ experiments was approximately 10 ns. The pump and probe laser beams were lightly focused onto the flowing sampling system, and the Raman light was collected using reflective optics into a spectrometer whose grating dispersed the light onto a liquid nitrogen cooled CCD detector. The Raman signal was accumulated for 30 s by the CCD before reading out to an interfaced PC computer and 10–20 scans of the signal were added together to get a resonance Raman spectrum. The ns-TR³ spectra presented here were obtained by the subtraction of a resonance Raman spectrum with negative time delay of −100 ns (probe-before-pump spectrum) from the resonance Raman spectrum with a positive time delay (pump–probe spectrum) and the Raman shifts were calibrated by the

known MeCN solvent Raman bands with an estimated accuracy of 5 cm^{-1} .

Density Functional Theory (DFT) Computations. DFT calculations were performed by the Becke three-parameter hybrid method with Lee–Yang–Parr correlation functional approximation (U) B3LYP method with a 6-31G(d,p) basis set.^{45,46} Raman spectra were obtained by determination of the Raman intensities from transition polarizabilities calculated by numerical differentiation with an assumed zero excitation frequency. A Lorentzian function with a 15 cm^{-1} bandwidth for the vibrational frequencies and a frequency scaling factor⁴⁷ of 0.986 was used for comparison between calculated results and the experimental spectra. No imaginary frequency modes were observed at the stationary states of the optimized structures, and only one imaginary frequency was observed for the saddle point transition state structures. The hydrogen transfer process was explored by optimizing the structures of the reactants, transition states, and product complexes. Transition states were located by using a Berny algorithm.⁴⁸ Frequency calculations at the same level of theory were performed to confirm that the structures were at local minima with all-real frequencies or at transition states with only one imaginary frequency. The nature of the transition states was determined by analyzing the motion by the eigenvector associated with the imaginary frequency. Intrinsic reaction coordinates (IRC)^{49–51} were calculated for the transition states to confirm the relevant structures connecting the two relevant minima. TD-DFT methodology was used to compute the low-lying excited states of transient species of interest.⁵² GaussSum software was utilized to simulate the UV–vis spectra.⁵³ The polarizable continuum model (PCM) was used for evaluating the (bulk) solvent effect.⁵⁴ All of the calculations were done using the Gaussian 03 program⁵⁵ installed in the High Performance Computing Cluster at the Computer Centre in The University of Hong Kong.

■ RESULTS AND DISCUSSION

UV/Vis Absorption and Resonance Raman Spectroscopic Study of the Ground-State of Fp in Acetonitrile. UV/vis absorption spectra can provide information about what species are excited at different excitation wavelengths and help in choosing suitable wavelength(s) for the pump laser pulse in time-resolved experiments. Ground-state resonance Raman spectroscopy can be employed to gain more detailed information about the nature of the species that contribute to the absorption spectra. The UV/vis absorption spectrum of Fp recorded in pure MeCN in the wavelength region between 220 and 320 nm shows a maximum at 245 nm with a shoulder band at around 278 nm (see Figure 3).

TD-DFT and frontier orbitals calculations were performed at the B3LYP/6-31G(d,p) theory level (see Figure 1S and Table 1S in the Supporting Information), and these results indicate that the two major absorption bands in the UV/vis spectrum are all characteristic of $\pi\pi^*$ absorption transitions with varying distributions of the highest occupied molecular orbital (HOMO) to lowest unoccupied molecular orbital (LUMO). The weaker band at 278 nm primarily is associated with the transitions from the HOMO to the LUMO and corresponds to the first vertical excitation. The stronger band at 245 nm is mainly associated with the transitions from HOMO-1 and HOMO-2 to the LUMO and corresponds to the second and third vertical excitations (see Figure 2S in the Supporting Information for details). Previously, Eriksson and co-workers

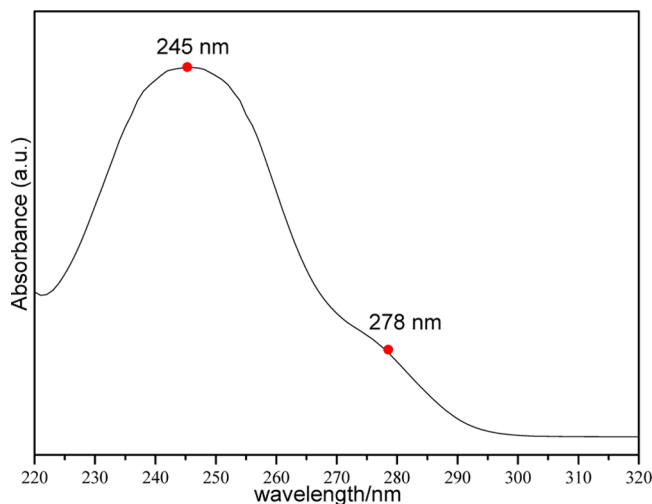


Figure 3. UV/vis absorption spectrum of Fp obtained in pure MeCN.

also performed similar calculations and found similar results.⁴² Based on the above analysis, it can be inferred that a pump laser with a 267 nm wavelength will excite the Fp molecule to its second excited singlet state S_2 .⁵⁶

To verify which forms of Fp are present in MeCN solvent, resonance Raman spectroscopy experiment was performed. Figure 4 shows the resonance Raman spectrum obtained for Fp

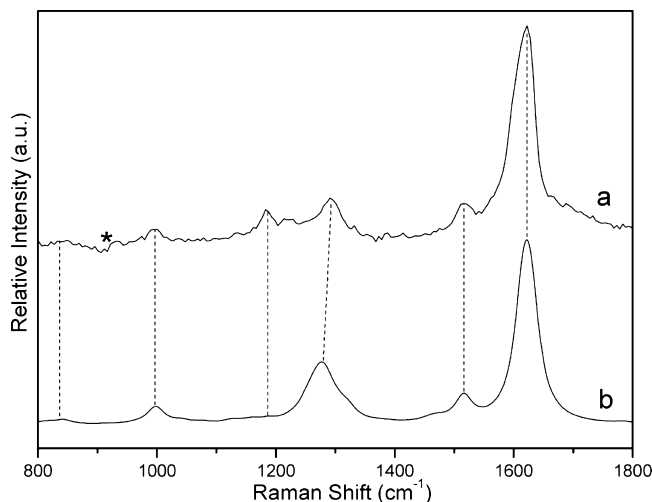


Figure 4. Comparison of (a) the resonance Raman spectrum of Fp obtained in pure MeCN with (b) the calculated ground-state normal Raman spectrum of Fp. The asterisks mark regions affected by solvent subtraction artifacts and/or stray light.

in MeCN compares with the predicted normal Raman spectrum computed at the B3LYP/6-31G(d,p) level of theory. Very good agreement between the experimental resonance Raman spectrum and the calculated normal Raman spectrum vibrational frequencies is observed and indicates the neutral Fp species is the main species associated with the UV absorption bands in MeCN. Most of the resonance Raman bands observed for Fp in the $800\text{--}1800\text{ cm}^{-1}$ region are associated with vibrations involving the ring C=C stretching, C–C stretching, and C=O stretching motions. For example, the C–C stretching and C=O stretching modes contribute to the Raman bands at 1622 and 1183 cm^{-1} . The ring-breathing vibrational motions contribute to the 996 cm^{-1} Raman band.

Further information about the comparison and assignments of the vibrational motions to the Raman bands is given in Table 2S of the Supporting Information.

The optimized structures of Fp in the ground state (S_0), the lowest lying excited singlet (S_1), and the lowest lying excited triplet (T_1) calculated at the (U) B3LYP/6-31G(d,p) level of theory are shown in Figure 5 (see Supporting Information for

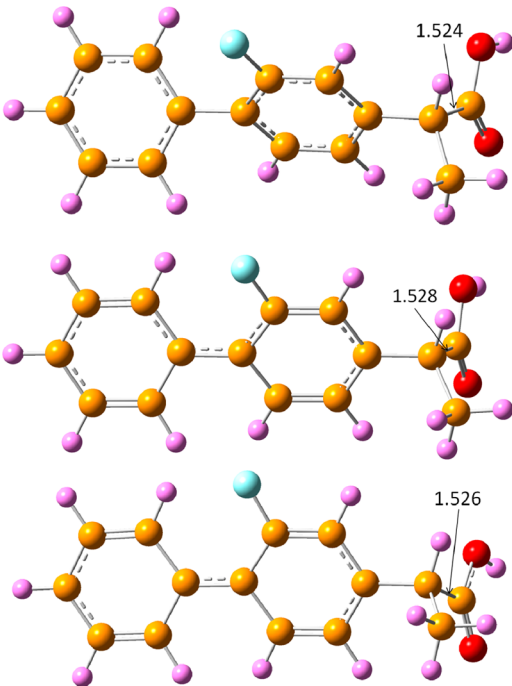


Figure 5. Optimized geometries of Fp involved with the S_0 (top), S_1 (middle), and T_1 (bottom) states are shown.

details). Inspection of Figure 5 reveals significant differences in the $C_{14}-C_{16}$ bond lengths (see Figure 1 for the label numbers) for the S_0 , S_1 , and T_1 states which are 1.524, 1.528, and 1.526 Å, respectively. Obviously, S_1 possesses the longest bond length for the $C_{14}-C_{16}$ bond and correspondingly the weakest bond energy for this bond of these states. Compared with the structure of the ground state, those of the excited states have very small dihedral angles between the two benzene rings and the C_6-C_7 bond has typical double bond character. Similarly, in the two benzene rings the proportions of the double bonds are inclined to increase. In summary, it can be concluded that Fp may prefer to decarboxylate from the S_1 state instead of the T_1 state in so far as the relevant $C_{14}-C_{16}$ bond is weaker in that state than in T_1 .

Fs-TA Spectroscopic Investigation of the Early Time Photophysics and Photochemistry. Figure 6 displays the fs-TA spectra of Fp obtained in pure MeCN from 0 to 3300 ps. To clearly indicate the spectral changes at different time scales, the spectra of early (0.2–1 ps) and late (after 2 ps) delay times are presented separately. Examination of Figure 6a reveals that a small band below 350 nm has appeared before 0.2 ps which can be reasonably assigned to the second excited singlet S_2 based on the UV-vis spectrum and relative TD-DFT calculations discussed in the preceding section. Subsequently, this band grew rapidly with a red shift to 374 nm accompanied by the appearance of a new band observed at around 420 nm whose relative intensity exceeds that at 374 nm. These two bands are tentatively assigned to the same species, denoted as

A. Furthermore, as can be seen from Figure 6b, after 2 ps the absorption band at 420 nm begins to decrease gradually while a reverse tendency displayed by the absorption band at 374 nm occurs; that is, a conspicuous growth was observed along with a slight blue shift to 367 nm. This indicates that one or more than one new species, denoted as B, having absorption at 367 nm was/were formed at the expense of the species A based on the presence of an isosbestic point located between 367 and 420 nm.

The band situated at about 350 nm has been assigned to S_2 . Generally, the higher excited state is very unstable and is prone to decay to the lower level through an internal conversion (IC) process. We tentatively assign the species A to be the lowest lying excited singlet S_1 state and the observed time scale for the apparent S_2 to S_1 conversion is consistent with an IC photophysical process time scale.⁵⁷ Because of the relatively high efficiency of ISC of up to 0.71,⁴⁰ the subsequent process in the spectral evolution is tentatively attributed to ISC from S_1 to T_1 . Unexpectedly, when we carried out the fitting of the kinetics of the absorption band at 368 nm we found that a simple biexponential function cannot fit the experimental data very well whereas a triexponential decay function provided a much better fit to the experimental kinetics (this fit is shown in Figure 7) obtained. The three time constants from this triexponential function fitting are $\tau_1 = 282$ fs, $\tau_2 = 50$ ps, and $\tau_3 = 1591$ ps, respectively. The rise time constant of $\tau_1 = 282$ fs is assigned to the IC process from S_2 to S_1 since it is consistent with the typical IC time scale. Since a triexponential function was needed to fit the kinetics well, this suggests that another process may take place in competition with the ISC process from the S_1 state. Consequently, we tentatively assigned the only decay time constant of $\tau_2 = 50$ ps to the ISC process and the rise time constant of $\tau_3 = 1591$ ps to another process that generates a minor species with a low quantum yield. These assignments are consistent with results for similar photophysical and photochemical time scales of other related compounds^{32,56,58} and the quantum yield for ISC (0.71 in MeCN) and photodegradation (<0.005 in organic solvents) for Fp.⁴⁰ For a Norrish reaction, the substrate may undergo a homolysis reaction in an inert solvent^{51,59} and an analogous homolysis reaction was proposed to proceed for Fp in MeCN to generate two radical species. Results from DFT calculations (see Figure 5) for the cleavage of the α -carbon bond located at $C_{14}-C_{16}$ gives rise to the COOH group leaving as a radical and the other part of the molecule is denoted as the FpR radical (see Scheme 2).

The DFT computations indicate that the homolysis cleavage occurring from the S_1 state of Fp will likely take place very fast. The $C_{14}-C_{16}$ bond was scanned outward from the optimized S_0 value (1.524 Å) in steps of 0.1 Å. At each new point, the structures were reoptimized, and the vertical excitation energies were calculated. The resulting energy curves obtained at the TD-B3LYP/6-31G(d,p) level of theory are displayed in Figure 8. The lowest excited singlet state surfaces are exothermic throughout the scan, and hence it can be concluded that homolytic photodecarboxylation is very likely to occur from the S_1 state of Fp. Similar computational investigations on nonsteroidal anti-inflammatory drugs, such as ketoprofen and ibuprofen, have also been reported by Eriksson and co-workers.^{42,60–64}

Additional computations were done to estimate the absorption spectra of T_1 and the FpR radical. Figure 9 presents the results for the absorption spectra of T_1 and the FpR radical

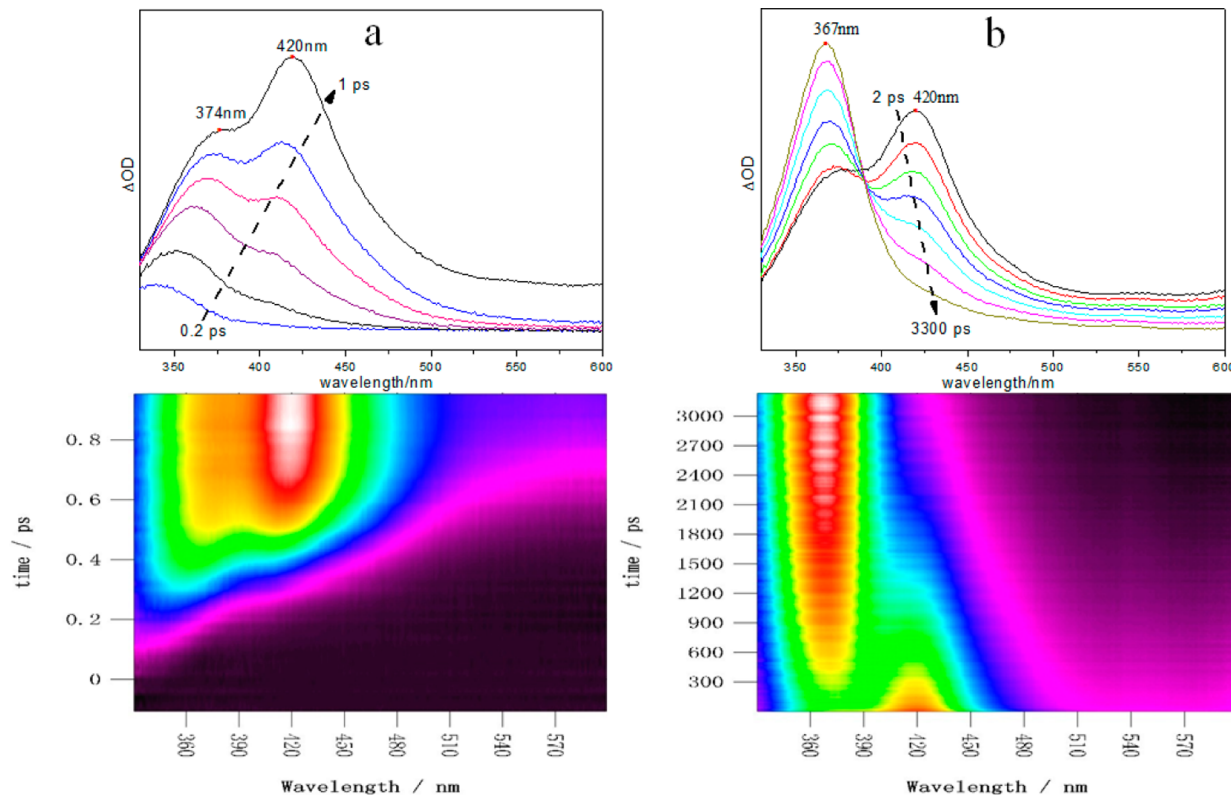


Figure 6. Fs-TA contours of Fp obtained at 267 excitation in pure MeCN accompanied with spectra in different delay times (a) 0–1 ps and (b) 2–3300 ps.

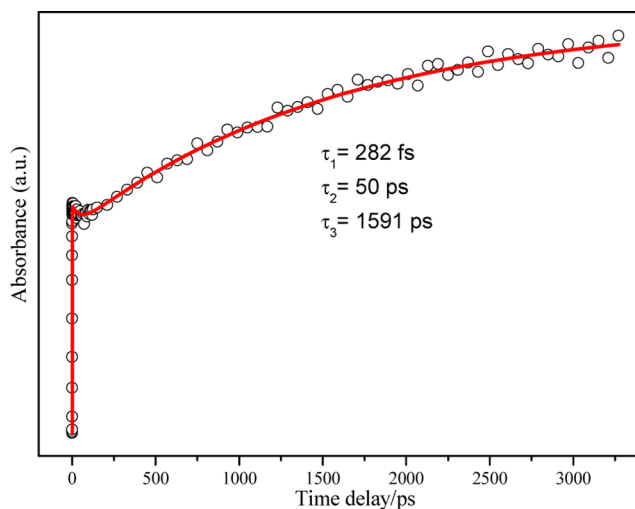
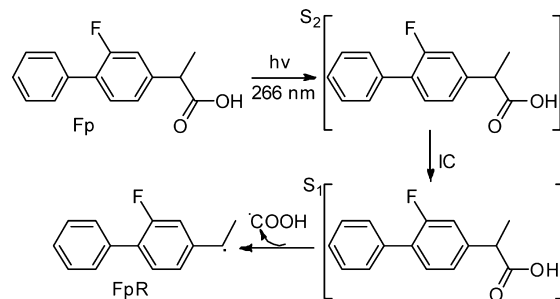


Figure 7. Experimental kinetics data at 368 nm (circles) of Fp obtained in MeCN with a triexponential function fit to the data (the red line represents the best fit).

derived from TD-DFT calculations done at the UB3LYP/6-31G(d,p) level of theory with consideration of the solvation effect by means of a PCM using UFF radii (see Tables 3S and 4S in the Supporting Information). The calculated spectra were drawn using GaussSum 2.2 software with a fwhm of 1500.⁵³ Inspection of Figure 9 reveals that the predicted T₁ and FpR radical spectra have two major absorption bands at 351 and 327 nm, respectively. It should be taken into consideration that the current level of theory is well-known to predict too high excitation energies by approximately 0.2 eV.⁶⁰ Accordingly, the computed spectra can be considered as being blue-shifted

Scheme 2. A Proposed Homolysis Photodecarboxylation Mechanism for the S₁ State



relative to the experiments by approximately 10–30 nm. These results are reasonably consistent with the fs-TA experimental results and provide additional support for the generation of the T₁ and the FpR radical species.

Ns-TA Spectroscopic Investigation of Intermediates Derived from Oxidation of the Radical Species. Although a rough scheme for the early time delay period photophysics and photochemistry was elucidated from the fs-TA spectra, the later time developments for the reaction pathways of the intermediates from the homolytic photodecarboxylation need to be elaborated further and we performed ns-TA spectroscopy experiments to examine the processes taking place from nanoseconds to microseconds. Figure 10 exhibits the ns-TA spectra gained in MeCN excited by 266 nm laser under nitrogen-saturated and oxygen-saturated conditions along with the delay times. The profiles of both spectra at 0 ns delay time, characterized by a major absorption band at 374 nm and a small shoulder at 440 nm, resemble the late delay time fs-TA spectra,

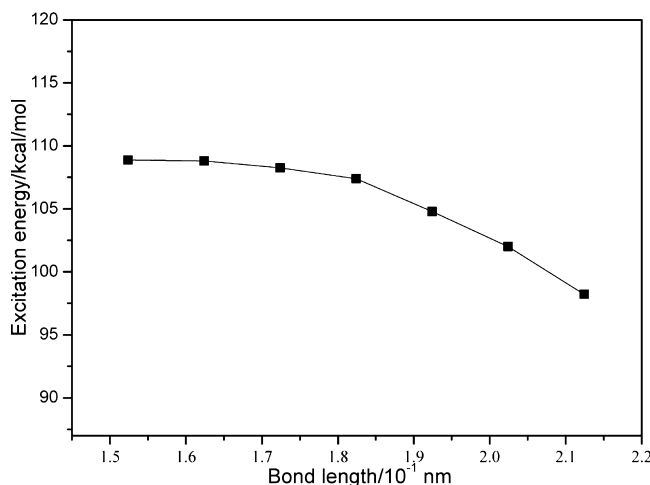


Figure 8. Energy curves of the lowest excited singlet states (S_1) for the decarboxylation of the neutral Fp molecule.

indicating that they should be due to the same transient species. As time evolves, there is an obvious increase in intensity for the absorption band at 440 nm from 0 to 25 ns for the spectra acquired under an oxygen-saturated condition (see Figure 10b). Subsequently, the absorption band at 440 nm begins to decrease in intensity piecemeal together with the band at 374 nm. In contrast, there is little change observed in the spectra obtained under a nitrogen-saturated condition. Together, these observations (see Figure 10, a and b) indicate that oxygen remarkably quenches the intermediates and these intermediates are likely triplet and/or radical species.⁵⁷ We tentatively assigned the major band at 374 nm to the triplet Fp species in the previous section and this is consistent with the relative intensity of the corresponding absorption band under an oxygen-saturated condition being lower in intensity than that under a nitrogen-saturated condition (see Figure 10a). Simultaneously, there should not be a new transient species generated as a result of quenching by oxygen of this triplet Fp species since it would be deactivated to return to the S_0 ground state. However, the experimental results show that there is an obvious growth in the absorption band at 440 nm due to formation of another species. In the light of that, it appears that the species quenched by oxygen is not a triplet species but may be a radical species that forms from the homolytic photo-

decarboxylation reaction. The decarboxylated product FpR radical can be oxidized by one oxygen molecule to give a new radical species that is denoted here as the FOR radical intermediate that has an absorption band at 440 nm (see Scheme 3). This can explain the formation of the new absorption band located at 440 nm. TD-DFT calculations were done at the UB3LYP/6-31G(d,p) level of theory to predict the absorption spectrum of the FOR species. The simulated calculated absorption spectrum was drawn by using the GaussSum 2.2 software with a fwhm of 4000 cm^{-1} ⁵³ and is shown in Figure 11 (see also the data of Table S5 in the Supporting Information). The strong absorption band predicted at 463 nm for the FOR radical is in reasonable agreement with the strong absorption band experimentally observed at 440 nm considering the expected uncertainty of the TD-DFT computations mentioned earlier. This provides some support for the assignment of the new absorption band at 440 nm being due to the FOR radical intermediate formed from the reaction of the FpR radical with oxygen.

To better understand the transformation of the transient species produced after decarboxylation, the kinetics of the absorption bands at 374 and 440 nm in the spectra obtained under both nitrogen-saturated and oxygen-saturated conditions were also investigated. Unexpectedly, the absorption decay kinetics for the 374 nm band cannot be fitted satisfactorily by a single-exponential function, whereas a biexponential function appears to fit the kinetics of absorption band at 374 nm under both experimental conditions. Decay time constants of $\tau_1 = 4$ and $\tau_2 = 13\text{ }\mu\text{s}$ were obtained under the nitrogen-saturated experimental conditions and values of 68 and 227 ns were found under the oxygen-saturated experimental conditions (see Figure 12). Apparently, this absorption band was quenched greatly by oxygen to shorten the lifetimes of the intermediates associated with the 374 nm transient absorption substantially. This is similar to the fitting results for the fs-TA spectra in that there seems to be more than one transient species present. Both the fs-TA and ns-TA results are consistent with both the triplet Fp and FpR radical species being present and reacting with oxygen at different rates and hence two different decay kinetics are observed in the ns-TA experiments. Under the oxygen-saturated experimental conditions, the time constant of 68 ns is assigned to the lifetime of T_1 based on that oxygen quenching of triplets is usually 4/9 of the rate constant of diffusion,⁶⁵ and the longer time constant of 227 ns is ascribed

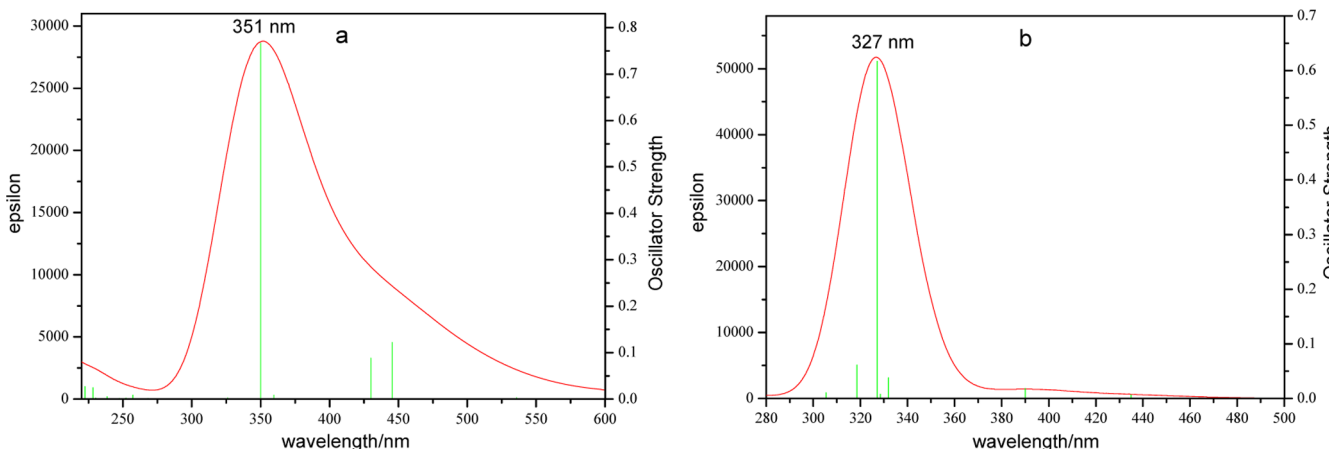


Figure 9. Calculated absorption spectra of (a) T_1 and (b) the FpR radical species.

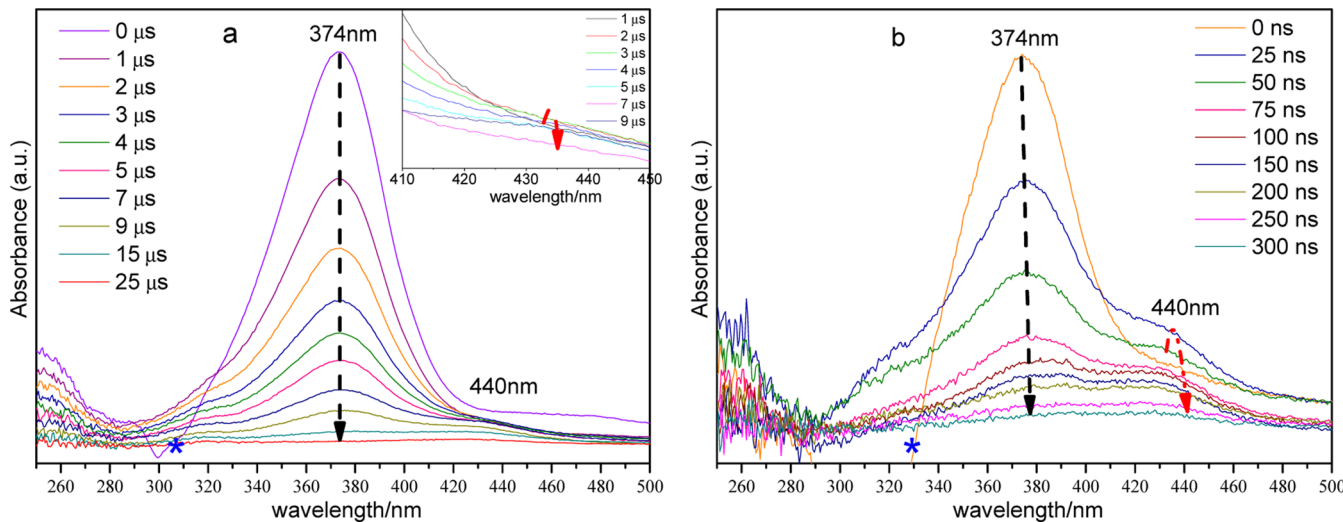


Figure 10. Ns-TA spectra of Fp obtained in pure MeCN (a) under nitrogen-saturated and (b) under oxygen-saturated condition. The asterisks mark regions affected by fluorescence emission.

Scheme 3. Oxidation Mechanism of the Photoinduced Decarboxylated Product FpR Radical Species to Produce the FOR Radical Species

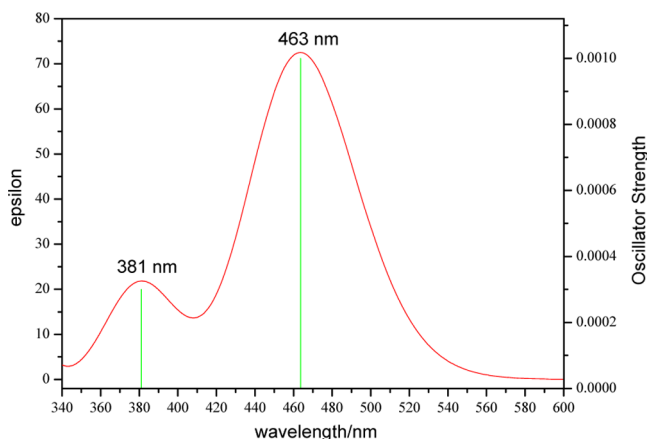
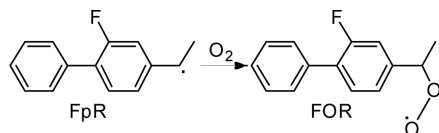


Figure 11. Calculated simulated absorption spectra of FOR.

to the radical species. Correspondingly, the time constants of 4 and 13 μ s obtained under nitrogen-saturated experimental conditions are assigned to the T₁ and FpR radical species, respectively. The kinetics of the absorption band at 440 nm that is assigned to the oxidation product of the FpR radical were fitted with a single-exponential function under both experimental conditions, and time constants of 10 μ s and 394 ns were found. It should be noted that there is still some oxygen remaining under the nitrogen-saturated experimental conditions due to the limitations of the experimental apparatus and therefore a small amount of oxidation product can also be detected under this experimental condition.

Ns-TR³ Spectra and DFT Calculations to Identify and Characterize the Reaction Intermediates. In previous studies, photoinduced decarboxylation was found to be an

efficient and general reaction for different types of arylcarboxylic acids in aqueous solutions at pH > pK_a⁶⁶ but few investigations reported that the decarboxylation reaction is able to proceed in MeCN other than the Fp molecule examined here. The fs-TA and ns-TA results in the preceding sections have elucidated a decarboxylation mechanism for Fp in MeCN but the assignments of the transient absorption bands of the intermediates are tentative in nature since the absorption bands are broad and featureless and not very diagnostic of the structure and identity of the intermediates. To obtain structural information and to clearly identify the intermediates associated with the transient absorption bands observed in the TA experiments, ns-TR³ experiments were performed to characterize several transient species observed in the photochemistry of Fp in MeCN. Figure 13 displays ns-TR³ spectra obtained by using a 266 nm pump laser pulse and a 416 nm probe laser pulse for a ~3 mM Fp in MeCN with the time delays between the pulses indicated next to each spectrum.

Inspection of Figure 13 shows that two species are generated within 5 μ s based on the results of the different decay rates for the Raman bands at 1467 and 1500 cm⁻¹, respectively. From the analysis of the fs-TA and ns-TA results, the excited singlet state appears to be involved in the decarboxylation reaction and this is analogous to the decarboxylation of *o*-acetylphenylacetic acid.⁶⁷ Both the ISC process and the fluorescence emission observed are consistent with the experimental quantum yields of 0.71 for ISC and 0.20 for fluorescence emission, respectively,⁴⁰ and this is the reason for the low quantum yield for the novel Fp decarboxylation reaction. In order to further study the identity and structure of the transient species from the decarboxylation reaction, calculations predicting the optimized geometry and vibrational frequencies for the species of interest were performed. The fs-TA and ns-TA spectra along with the TD-DFT predicted absorption spectra tentatively assigned two transient species derived from the excited singlet state to a triplet Fp intermediate (T₁) and a coexisting radical intermediate (FpR) species. The normal Raman spectra of these T₁ and FpR intermediates were computed and compared with the ns-TR³ spectrum obtained in MeCN at a 0 ns delay time as shown in Figure 14. Examination of Figure 14 reveals that the Raman band at 1580 cm⁻¹ is characteristic of the FpR intermediate as well as the Raman bands located at 1462 and

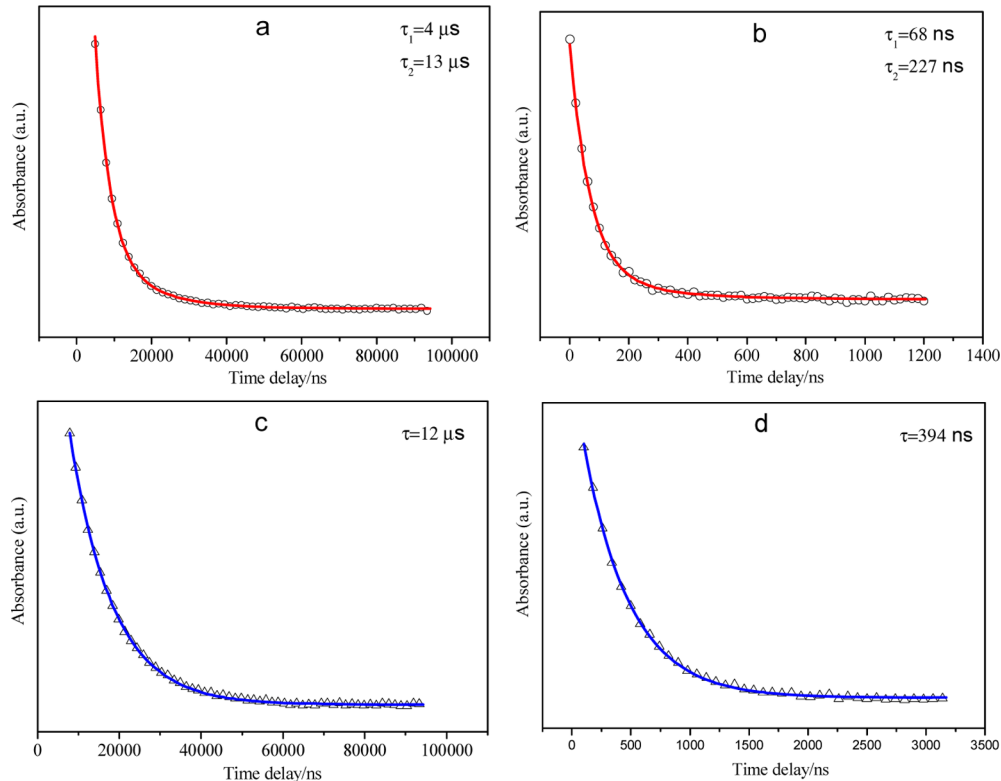


Figure 12. Ns-TA kinetics with its fitting plots: (a) at 373 nm and (c) at 435 nm under nitrogen-saturated condition; (b) at 373 nm and (d) at 435 nm under oxygen-saturated condition.

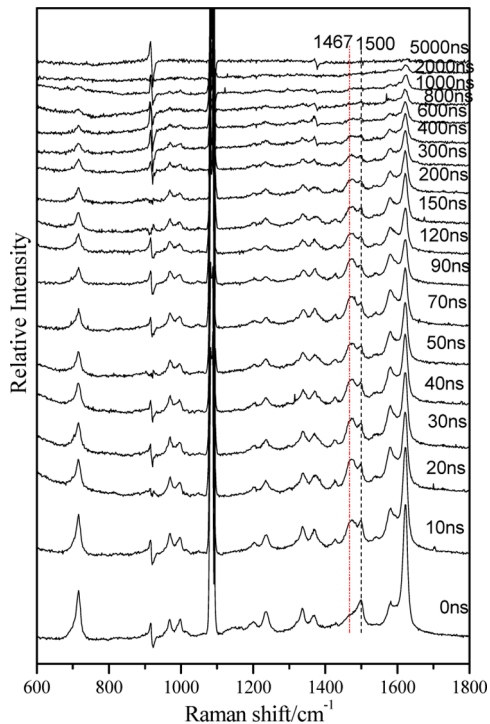


Figure 13. Shown are ns-TR³ spectra of 3 mM Fp in pure MeCN obtained using a 266 nm pump wavelength and a 416 nm probe wavelength.

998 cm⁻¹. The Raman bands situated at 1429, 1336, 1236, and 967 cm⁻¹ are assigned to T₁. The Raman bands at 1621, 1500, 1369, 1201, and 716 cm⁻¹ have contributions from both the T₁ and FpR intermediates.

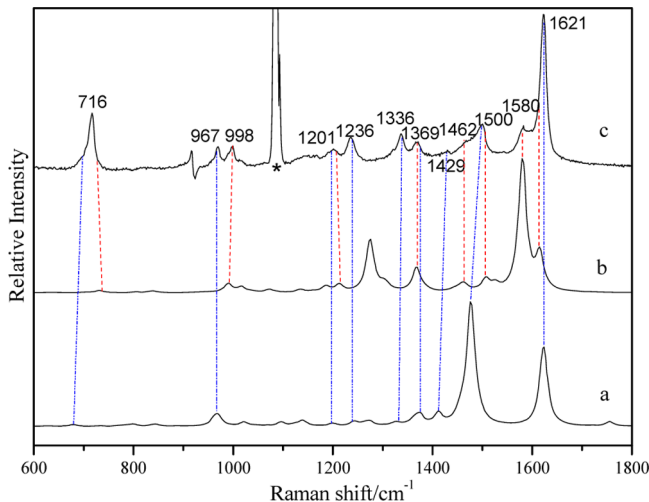


Figure 14. Comparison of the (c) experimental ns-TR³ spectrum of Fp in pure MeCN acquired at a time delay of 0 ns with the DFT calculated spectra for the (a) T₁ and (b) FpR intermediates. The asterisk (*) symbols mark subtraction artifacts.

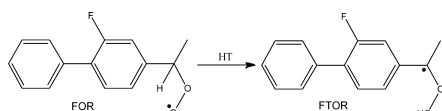
With regard to the assignments of the different Raman bands, only a very brief description will be given here and the reader is referred to Table 6S in the Supporting Information for a detailed comparison of the experimental ns-TR³ vibrational frequencies to the corresponding calculated vibrational frequencies for the T₁ and the FpR intermediates. Most of the Raman bands observed for the T₁ species are due to the vibrations associated with the C–C stretch motions of the phenyl rings. For example, the Raman bands at 849, 1329, 1355, and 1575 cm⁻¹ are mainly due to these kinds of

vibrational modes. The Raman band at 1171 cm^{-1} has contributions not only from the C–C stretch motions but also from a C–H bend motion.

Most of the Raman bands disappear at long time delays, and no other new Raman bands were generated so that only the Raman band at 1621 cm^{-1} due to the T_1 species is observed on the tens of microseconds time scale in Figure 13. The T_1 does not seem to be involved in the decarboxylation reaction of Fp and hence it has a longer lifetime. In contrast, the FpR intermediate is a highly reactive species which is prone to be oxidized in the presence of oxygen, so it decayed more rapidly in the ns-TR³ and ns-TA spectra. Based on that, it can be regarded that the Raman band at 1621 cm^{-1} in the later time delay spectra is mainly due to the T_1 species. Although the oxidized product from the reaction of FpR and oxygen has a major absorption band at about 440 nm (see ns-TA spectra), the decarboxylation reaction quantum yield is so low that it is cannot be easily detected in the ns-TR³ experiments. This is why no new Raman bands were observed at later time delays from the reaction of the FpR intermediate with oxygen. DFT calculations were done to help understand the steps from the observed intermediates to the final products 1 and 2.

It is widely accepted that the radical species can be easily oxidized by oxygen to produce a peroxy radical. In the present case, the oxidized product of FpR will be denoted as FOR which can then undergo a swift hydrogen transfer (HT) due to the tertiary hydrogen being adjacent to the reactive oxygen molecule that can make the carbonic radical which will be denoted as FTOR here (see Scheme 4). The potential energy

Scheme 4. Hydrogen Transfer Mechanism of the FOR Radical To Produce the FTOR Radical



surface (PES) of this unimolecular reaction was explored to locate a viable pathway for the HT process from the FOR radical to the FTOR radical. The stationary points (minima and transitions states, TSs) were located in the gas phase.

There are two possible pathways for the FOR radical to undergo the HT process to the FTOR radical. The first pathway is a two-step reaction that involves a dehydrogen (DH) step and a hydrogen abstraction (HA) step. DFT calculations done at the UB3lyp/6-31G(d,p) level of theory to explore this pathway and internal reaction coordinate forward and reverse (IRCF and IRCR) computations were performed to ascertain the appropriate reactants, TSs, and products connected along the pathway. The optimized structures obtained for the reactant complex (RC_x), transient state (TS_x), and product complex (PC_x) of the two-step reaction pathway are shown in Figure 3S in the Supporting Information. The relative energy profiles obtained from the reaction pathway calculations are displayed in Figure 15. Inspection of Figure 15 indicates that the activation energy for the HT process through the two-step pathway (62.9 kcal/mol) is so high that the reaction is highly unlikely to proceed via this pathway. A reasonable explanation is that the dehydrogen step gives rise to an unstable hydrogen atom that causes the whole system to be in a relative higher energy state so that the activation energy is very high. Based on that, a different one-step reaction is

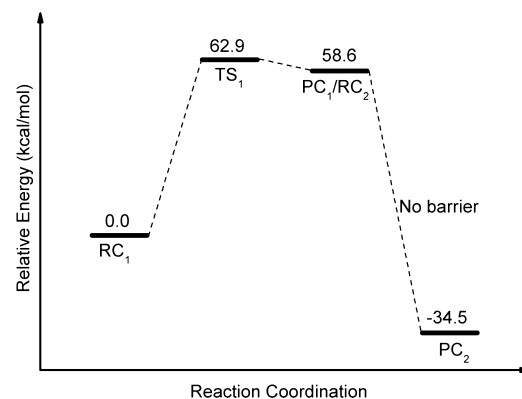


Figure 15. Reactive energy profile obtained from the DFT calculations for HT process involving two steps.

considered in which the DH and HA take place simultaneously to eliminate the unstable hydrogen atom that is abstracted by the adjacent oxygen atom. Similarly, the optimized structures obtained for the RC, TS, and PC of the one-step reaction pathway are shown in Figure 4S in the Supporting Information. The relative energy profiles obtained from the reaction pathway calculations are displayed in Figure 16. In expectation, the

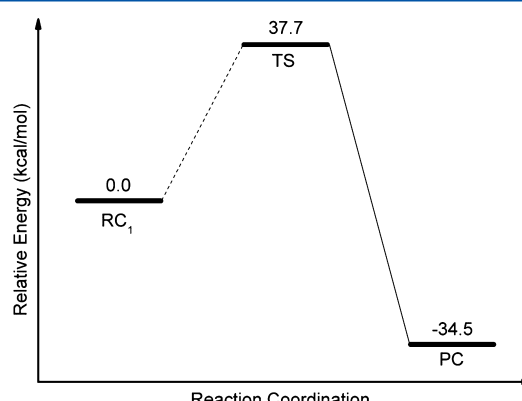


Figure 16. Reactive energy profile obtained from the DFT calculations for HT process involving one step.

activation energy decreases greatly to 37.7 kcal/mol, but it is still somewhat higher than that (20 kcal/mol) for a typical viable photochemical reaction.⁵¹ The Mulliken spin distribution of the TS (see Figure 17 and Table 7S in the Supporting Information) was examined to determine the spin located on the leaving hydrogen atom and the oxygen atom receiving the hydrogen atom and these results also indicate that this reaction

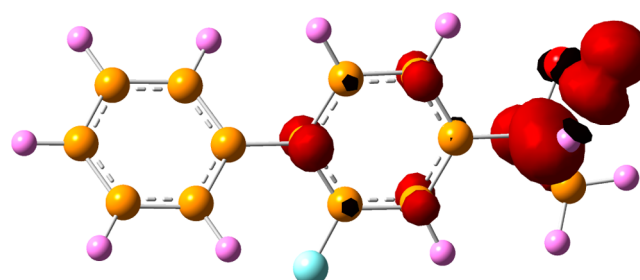
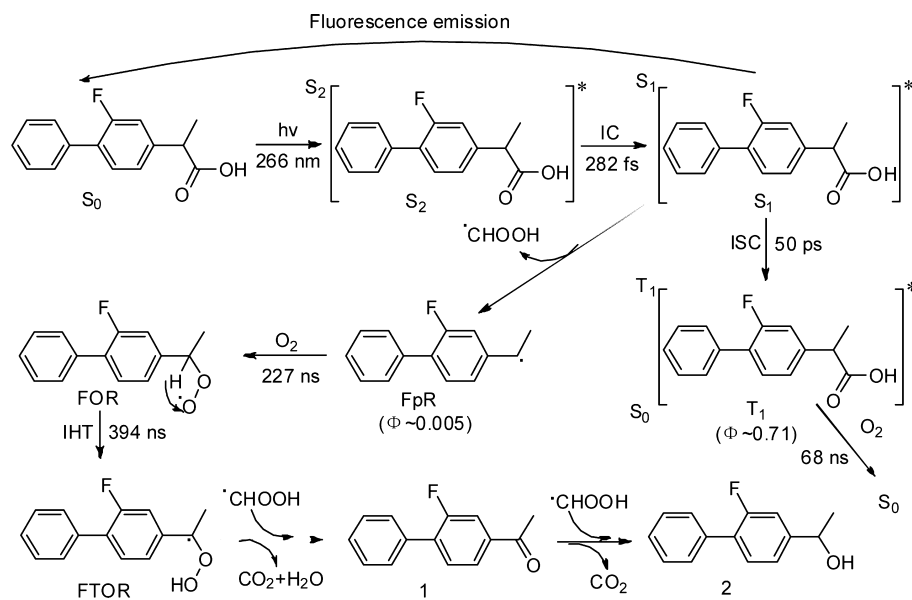


Figure 17. Mulliken spin distribution for the TS calculated at the UB3LYP/6-31G(d,p) level of theory.

Scheme 5. Proposed Reaction Mechanism for the Ultraviolet Excitation of Fp in Pure MeCN Based on the Direct Time-Resolved Spectroscopy Observations and DFT Computational Results



is a homolytic one that needs a high activation energy in general. Therefore, the activation energy still appears to be too high. The final product **1** can be formed by spontaneous dehydroxylation accompanying the hydrogen transfer process.

However, we do not exclude the viability of this reaction pathway, because it is possible that a proton-coupled electron-transfer (PCET) process takes part in the reaction to give a HT with a lower activation energy. It has been extensively established for PCET as early as 2007 that the proton transfer generally requires a lower activation energy than a hydrogen transfer when it proceeds with an accompanying electron transfer.^{68–74} Such a mechanism can be rationally applied in the present system so that the activation energy produced by deprotonation is inclined to be lower than that generated by dehydrogenation and therefore allows the reaction to take place with a reasonable activation barrier. Thus, it appears viable that the system of interest here can undergo a hydrogen-transfer process to result in spontaneous dehydroxylation to produce the final product **1**. The other final product **2** may be formed by addition of a hydroxyl arising from the leaving group COOH radical of the FpR radical. Since product **2** was only found with a trace quantum yield,⁴⁰ it will not be discussed further here.

CONCLUSION

A novel photodecarboxylation that involves the homolysis of the carbon α -bond of Fp in its excited singlet state was characterized using time-resolved spectroscopic experiments (including fs-TA, ns-TA and ns-TR³ spectroscopy) and results from DFT calculations. Fs-TA experiments examined the initial photophysics and reactive intermediates. The first transient species detected had a strong absorption band at about 350 nm that was assigned to the S₂ excited state produced by the initial photoexcitation of the ground-state Fp molecule. Subsequently, a new strong absorption band appeared at 420 nm and is associated with the generation of the S₁ excited state via IC from S₂. Interestingly, S₁ may decay via fluorescence emission back to the ground state or via ISC to form the T₁ intermediate, or undergo a low quantum yield decarboxylation reaction to form a radical species (FpR). In the subsequent reactions,

oxygen acted to oxidize the FpR intermediate to form another radical species (FOR), which was directly observed and characterized by ns-TA spectra obtained under oxygen-saturated and nitrogen-saturated experimental conditions. The TR³ spectra supplied important fingerprint evidence for the assignments of some of the key transient species. The time-resolved spectroscopy results in conjunction with results from DFT calculations were used to elucidate the photophysics and reaction mechanisms associated with the photochemistry of Fp in MeCN solution which is shown in Scheme 5. This work has helped gain further insight into the unusual photodecarboxylation reaction of the Fp molecule observed in MeCN solvent.

ASSOCIATED CONTENT

Supporting Information

The TD-DFT predicted absorption spectrum of the ground state of Fp is shown. The DFT calculated frontier orbitals of the ground state Fp involved in the HOMO-2, HOMO-1, HOMO, and LUMO orbitals are shown. The optimized geometries of the RC, TS, and PC obtained from the DFT calculations for the reaction of hydrogen transfer are provided. The DFT Mulliken spin distribution of the TB³ species are given. The excited-state energies and oscillator strengths determined from the DFT calculations are shown for the ground state Fp, triplet Fp (T₁), FpR, and FOR intermediates. Comparisons of the experimental resonance Raman or ns-TR³ spectra vibrational frequencies with the DFT calculated vibrational frequencies for the T₁ and FpR intermediates with preliminary vibrational assignments and qualitative descriptions of the vibrational modes in the 800–1800 cm⁻¹ region are presented. The Cartesian coordinates used in the calculations of all the intermediates are provided. This material is available free of charge via the Internet at <http://pubs.acs.org>.

AUTHOR INFORMATION

Corresponding Author

*Fax: (+852) 2597-1586. Tel.: (+852) 2859 2160. E-mail: phillips@hku.hk

Notes

The authors declare no competing financial interest.

ACKNOWLEDGMENTS

This work was supported by a grant from the Research Grants Council of Hong Kong (HKU 7048/11P) and the University Grants Committee Special Equipment Grant (SEG-HKU-07) to D.L.P. Support from the University Grants Committee Areas of Excellence Scheme (AoE/P-03/08) is also gratefully acknowledged.

REFERENCES

- (1) Bass, J.; Athreya, B.; Brandstrup, N.; Brewer, E.; Dianni, M.; Goldsmith, D.; Hollister, R.; Kredich, D.; Miller, J. Flurbiprofen in the Treatment of Juvenile Rheumatoid-Arthritis. *J. Rheumatol.* **1986**, *13*, 1081–1083.
- (2) Preston, S. J.; Arnold, M. H.; Beller, E. M.; Brooks, P. M.; Buchanan, W. W. Variability in Response to Nonsteroidal Anti-Inflammatory Analgesics - Evidence from Controlled Clinical Therapeutic Trial of Flurbiprofen in Rheumatoid-Arthritis. *Br. J. Clin. Pharmacol.* **1988**, *26*, 759–764.
- (3) Kean, W. F.; Antal, E. J.; Grace, E. M.; Cauvier, H.; Rischke, J.; Buchanan, W. W. The Pharmacokinetics of Flurbiprofen in Younger and Elderly Patients with Rheumatoid-Arthritis. *J. Clin. Pharmacol.* **1992**, *32*, 41–48.
- (4) Rovensky, J.; Micekova, D. Six-Month Prospective Study to Monitor the Treatment of Rheumatic Diseases with Sustained-Release Flurbiprofen. *Drug Exp. Clin. Res.* **2000**, *26*, 19–24.
- (5) Tan, P.; Flowers, F. P.; Araujo, O. E.; Doering, P. Effect of Topically Applied Flurbiprofen on Ultraviolet-Induced Erythema. *Drug Intell. Clin. Pharm.* **1986**, *20*, 496–499.
- (6) Butler, R. C.; Goddard, D. H.; Higgens, C. S.; Hollingworth, P.; Pease, C. T.; Stodell, M. A.; Scott, J. T. Double-Blind Trial of Flurbiprofen and Phenylbutazone in Acute Gouty-Arthritis. *Br. J. Clin. Pharmacol.* **1985**, *20*, 511–513.
- (7) Stamp, J.; Rhind, V.; Haslock, I. A Comparison of Nefopam and Flurbiprofen in the Treatment of Osteoarthritis. *Br. J. Clin. Pract.* **1989**, *43*, 24–26.
- (8) Bellamy, N.; Bensen, W. G.; Ford, P. M.; Huang, S. H.; Lang, J. Y. Double-Blind Randomized Controlled Trial of Flurbiprofen-Sr (Ansaid-Sr(R)) and Diclofenac Sodium-Sr (Voltaren-Sr) in the Treatment of Osteoarthritis. *Clin. Invest. Med.-Med. Clin. Exp.* **1992**, *15*, 427–433.
- (9) Lagrue, G.; Laurent, J.; Thebault, J. J. Is Flurbiprofen Effective against Migrainous Attacks. *Presse Med.* **1983**, *12*, 901–901.
- (10) Mena, H. R.; Lomen, P. L.; Turner, L. F.; Lamborn, K. R.; Brinn, E. L. Treatment of Acute Shoulder Syndrome with Flurbiprofen. *Am. J. Med.* **1986**, *80*, 141–144.
- (11) Solomon, G. D.; Kunkel, R. S. Flurbiprofen in the Prophylaxis of Migraine. *Clev. Clin. J. Med.* **1993**, *60*, 43–48.
- (12) Moore, R. A.; Tramer, M. R.; Carroll, D.; Wiffen, P. J.; McQuay, H. J. Quantitative Systematic Review of Topically Applied Non-Steroidal Anti-Inflammatory Drugs. *Br. Med. J.* **1998**, *316*, 333–338.
- (13) Appiotti, A.; Gualdi, L.; Alberti, M.; Gualdi, M. Comparative Study of the Analgesic Efficacy of Flurbiprofen and Diclofenac in Patients Following Excimer Laser Photorefractive Keratectomy. *Clin. Ther.* **1998**, *20*, 913–920.
- (14) Vetrugno, M.; Maino, A.; Quaranta, G. M.; Cardia, L. A Randomized, Double-Masked, Clinical Study of the Efficacy of Four Nonsteroidal Anti-Inflammatory Drugs in Pain Control after Excimer Laser Photorefractive Keratectomy. *Clin. Ther.* **2000**, *22*, 719–731.
- (15) Bayly, C. I.; Black, W. C.; Leger, S.; Ouimet, N.; Ouellet, M.; Percival, M. D. Structure-Based Design of Cox-2 Selectivity into Flurbiprofen. *Bioorg. Med. Chem. Lett.* **1999**, *9*, 307–312.
- (16) Lanzo, C. A.; Sutin, J.; Rowlinson, S.; Talley, J.; Marnett, L. J. Fluorescence Quenching Analysis of the Association and Dissociation of a Diarylheterocycle to Cyclooxygenase-1 and Cyclooxygenase-2: Dynamic Basis of Cyclooxygenase-2 Selectivity. *Biochemistry* **2000**, *39*, 6228–6234.
- (17) Smith, T.; McCracken, J.; Shin, Y. K.; DeWitt, D. Arachidonic Acid and Nonsteroidal Anti-Inflammatory Drugs Induce Conformational Changes in the Human Prostaglandin Endoperoxide H-2 Synthase-2 (Cyclooxygenase-2) (Retracted Article. See Vol 279, Pg 6204, 2004). *J. Biol. Chem.* **2000**, *275*, 40407–40415.
- (18) Timofeevski, S. L.; Prusakiewicz, J. J.; Rouzer, C. A.; Marnett, L. J. Isoform-Selective Interaction of Cyclooxygenase-2 with Indomethacin Amides Studied by Real-Time Fluorescence, Inhibition Kinetics, and Site-Directed Mutagenesis. *Biochemistry* **2002**, *41*, 9654–9662.
- (19) Rahman, M. H.; Yamasaki, K.; Shin, Y. H.; Lin, C. C.; Otagiri, M. Characterization of High-Affinity Binding-Sites of Nonsteroidal Antiinflammatory Drugs with Respect to Site-Specific Probes on Human Serum-Albumin. *Biol. Pharmacol. Bull.* **1993**, *16*, 1169–1174.
- (20) Bosca, F.; Marin, M. L.; Miranda, M. A. Photoreactivity of the Nonsteroidal Anti-Inflammatory 2-Arylpropionic Acids with Photosensitizing Side Effects. *Photochem. Photobiol.* **2001**, *74*, 637–655.
- (21) Castell, J. V.; Gomezelchon, M. J.; Miranda, M. A.; Morera, I. M. Phototoxicity of Nonsteroidal Antiinflammatory Drugs - Invitro Testing of the Photoproducts of Butibufen and Flurbiprofen. *J. Photochem. Photobiol. B* **1992**, *13*, 71–81.
- (22) <http://www.drugs.com/sfx/flurbiprofen-side-effects.html>.
- (23) Kawada, A.; Aragane, Y.; Maeda, A.; Yudate, T.; Tezuka, T. Contact Dermatitis Due to Flurbiprofen. *Contact Dermatitis* **2000**, *42*, 167–168.
- (24) Encinas, S.; Miranda, M. A.; Marconi, G.; Monti, S. Triplet Photoreactivity of the Diaryl Ketone Tiaprofenic Acid and Its Decarboxylated Photoproduct. Photobiological Implications. *Photochem. Photobiol. Sci.* **1998**, *67*, 420–425.
- (25) Encinas, S.; Miranda, M. A.; Marconi, G.; Monti, S. Triplet Photoreactivity of the Diaryl Ketone Tiaprofenic Acid and Its Decarboxylated Photoproduct. Photobiological Implications. *Photochem. Photobiol.* **1998**, *67*, 420–425.
- (26) Vinette, A. L.; McNamee, J. P.; Bellier, P. V.; McLean, J. R. N.; Scaiano, J. C. Prompt and Delayed Nonsteroidal Anti-Inflammatory Drug-Photoinduced DNA Damage in Peripheral Blood Mononuclear Cells Measured with the Comet Assay. *Photochem. Photobiol. Sci.* **2003**, *77*, 390–396.
- (27) Ma, C. S.; Kwok, W. M.; Chan, W. S.; Du, Y.; Zuo, P.; Kan, J. T. W.; Toy, P. H.; Phillips, D. L. Time-Resolved Spectroscopy Studies of the Photodeprotection Reactions of P-Hydroxyphenacyl Ester Phototrigger Compounds. *Curr. Sci.* **2009**, *97*, 202–209.
- (28) Li, M. D.; Du, Y.; Chuang, Y. P.; Xue, J. D.; Phillips, D. L. Water Concentration Dependent Photochemistry of Ketoprofen in Aqueous Solutions. *Phys. Chem. Chem. Phys.* **2010**, *12*, 4800–4808.
- (29) Ma, C. S.; Kwok, W. M.; An, H. Y.; Guan, X. G.; Fu, M. Y.; Toy, P. H.; Phillips, D. L. A Time-Resolved Spectroscopic Study of the Bichromophoric Phototrigger 3',5'-Dimethoxybenzoin Diethyl Phosphate: Interaction between the Two Chromophores Determines the Reaction Pathway. *Chem.—Eur. J.* **2010**, *16*, 5102–5118.
- (30) Ma, J. N.; Cheng, S. C.; An, H. Y.; Li, M. D.; Ma, C. S.; Rea, A. C.; Zhu, Y.; Nganga, J. L.; Dore, T. M.; Phillips, D. L. Comparison of the Absorption, Emission, and Resonance Raman Spectra of 7-Hydroxyquinoline and 8-Bromo-7-Hydroxyquinoline Caged Acetate. *J. Phys. Chem. A* **2011**, *115*, 11632–11640.
- (31) Ma, J. N.; Li, M. D.; Phillips, D. L.; Wan, P. Reaction Mechanisms and Structural Characterization of the Reactive Intermediates Observed after the Photolysis of 3-(Hydroxymethyl)-Benzophenone in Acetonitrile, 2-Propanol, and Neutral and Acidic Aqueous Solutions. *J. Org. Chem.* **2011**, *76*, 3710–3719.
- (32) Li, M. D.; Ma, J. N.; Su, T.; Liu, M. Y.; Yu, L. H.; Phillips, D. L. Direct Observation of Triplet State Mediated Decarboxylation of the Neutral and Anion Forms of Ketoprofen in Water-Rich, Acidic, and PBS Solutions. *J. Phys. Chem. B* **2012**, *116*, 5882–5887.
- (33) Ma, J. N.; Rea, A. C.; An, H. Y.; Ma, C. S.; Guan, X. G.; Li, M. D.; Su, T.; Yeung, C. S.; Harris, K. T.; Zhu, Y.; et al. Unraveling the Mechanism of the Photodeprotection Reaction of 8-Bromo- and 8-

- Chloro-7-Hydroxyquinoline Caged Acetates. *Chem.—Eur. J.* **2012**, *18*, 6854–6865.
- (34) Dorman, G.; Prestwich, G. D. Benzophenone Photophores in Biochemistry. *Biochemistry* **1994**, *33*, 5661–5673.
- (35) Martinez, L. J.; Scaiano, J. C. Transient Intermediates in the Laser Flash Photolysis of Ketoprofen in Aqueous Solutions: Unusual Photochemistry for the Benzophenone Chromophore. *J. Am. Chem. Soc.* **1997**, *119*, 11066–11070.
- (36) Cosa, G.; Martinez, L. J.; Scaiano, J. C. Influence of Solvent Polarity and Base Concentration on the Photochemistry of Ketoprofen: Independent Singlet and Triplet Pathways. *Phys. Chem. Chem. Phys.* **1999**, *1*, 3533–3537.
- (37) David Budac, P. W. Photodecarboxylation: Mechanism and Synthetic Utility. *J. Photochem. Photobiol., A* **1992**, *67*, 135–166.
- (38) Li, M. D.; Yeung, C. S.; Guan, X. G.; Ma, J. N.; Li, W.; Ma, C. S.; Phillips, D. L. Water- and Acid-Mediated Excited-State Intramolecular Proton Transfer and Decarboxylation Reactions of Ketoprofen in Water-Rich and Acidic Aqueous Solutions. *Chem.—Eur. J.* **2011**, *17*, 10935–10950.
- (39) Encinas, S.; Miranda, M. A.; Marconi, G.; Monti, S. Transient Species in the Photochemistry of Tiaprofenic Acid and Its Decarboxylated Photoproduct. *Photochem. Photobiol. Sci.* **1998**, *68*, 633–639.
- (40) Jimenez, M. C.; Miranda, M. A.; Tormos, R.; Vaya, I. Characterisation of the Lowest Singlet and Triplet Excited States of S-Flurbiprofen. *Photochem. Photobiol. Sci.* **2004**, *3*, 1038–1041.
- (41) Chao, S. H.; Ho, H. T.; Chen, F. A.; Lin, P. Y.; Yu, Y. C.; Wu, A. B. Identification of Flurbiprofen and Its Photoproducts in Methanol by Gas Chromatography-Mass Spectrometry. *Biomed. Chromatogr.* **2007**, *21*, 527–533.
- (42) Musa, K. A. K.; Eriksson, L. A. Photochemical and Photophysical Properties, and Photodegradation Mechanism, of the Non-Steroidal Anti-Inflammatory Drug Flurbiprofen. *J. Photochem. Photobiol., A* **2009**, *202*, 48–56.
- (43) Srinivasan, A.; Kebede, N.; Saavedra, J. E.; Nikolaitchik, A. V.; Brady, D. A.; Yourd, E.; Davies, K. M.; Keefer, L. K.; Toscano, J. P. Chemistry of the Diazeniumdiolates. 3. Photoreactivity. *J. Am. Chem. Soc.* **2001**, *123*, 5465–5472.
- (44) Chan, P. Y.; Ong, S. Y.; Zhu, P. Z.; Zhao, C. Y.; Phillips, D. L. Transient Resonance Raman and Density Functional Theory Investigation of 4-Methoxyphenylnitrenium and 4-Ethoxyphenylnitrenium Ions. *J. Phys. Chem. A* **2003**, *107*, 8067–8074.
- (45) Lee, C. T.; Yang, W. T.; Parr, R. G. Development of the Colle-Salvetti Correlation-Energy Formula into a Functional of the Electron-Density. *Phys. Rev. B* **1988**, *37*, 785–789.
- (46) Becke, A. D. Density-Functional Thermochemistry 0.3. The Role of Exact Exchange. *J. Chem. Phys.* **1993**, *98*, 5648–5652.
- (47) Merrick, J. P.; Moran, D.; Radom, L. An Evaluation of Harmonic Vibrational Frequency Scale Factors. *J. Phys. Chem. A* **2007**, *111*, 11683–11700.
- (48) Schlegel, H. B. Optimization of Equilibrium Geometries and Transition Structures. *J. Comput. Chem.* **1982**, *3*, 214–218.
- (49) Cancès, E.; Mennucci, B.; Tomasi, J. A New Integral Equation Formalism for the Polarizable Continuum Model: Theoretical Background and Applications to Isotropic and Anisotropic Dielectrics. *J. Chem. Phys.* **1997**, *107*, 3032–3041.
- (50) Mennucci, B.; Tomasi, J. Continuum Solvation Models: A New Approach to the Problem of Solute's Charge Distribution and Cavity Boundaries. *J. Chem. Phys.* **1997**, *106*, 5151–5158.
- (51) Cossi, M.; Barone, V.; Mennucci, B.; Tomasi, J. Ab Initio Study of Ionic Solutions by a Polarizable Continuum Dielectric Model. *Chem. Phys. Lett.* **1998**, *286*, 253–260.
- (52) Runge, E.; Gross, E. K. U. Density-Functional Theory for Time-Dependent Systems. *Phys. Rev. Lett.* **1984**, *52*, 997–1000.
- (53) O'Boyle, N. M.; Tenderholt, A. L.; Langner, K. M. Cclib: A Library for Package-Independent Computational Chemistry Algorithms. *J. Comput. Chem.* **2008**, *29*, 839–845.
- (54) Tomasi, J.; Mennucci, B.; Cammi, R. Quantum Mechanical Continuum Solvation Models. *Chem. Rev.* **2005**, *105*, 2999–3093.
- (55) Frisch, M. J.; Trucks, G. W.; Schlegel, H. B.; Scuseria, G. E.; Robb, M. A.; Cheeseman, J. R.; Montgomery, J. A., Jr.; Vreven, T.; Kudin, K. N.; Burant, J. C.; et al. *Gaussian 03*; Gaussian, Inc.: Wallingford, CT, 2004.
- (56) Ma, C.; Kwok, W. M.; Chan, W. S.; Zuo, P.; Wai Kan, J. T.; Toy, P. H.; Phillips, D. L. Ultrafast Time-Resolved Study of Photophysical Processes Involved in the Photodeprotection of P-Hydroxyphenacyl Caged Phototrigger Compounds. *J. Am. Chem. Soc.* **2005**, *127*, 1463–1472.
- (57) Turro, N. J. *Modern Molecular Photochemistry*; University Science Books: Sausalito, CA, 1991.
- (58) Su, T.; Ma, J.; Li, M.-D.; Guan, X.; Yu, L.; Phillips, D. L. Time-Resolved Spectroscopic Study of the Photochemistry of Tiaprofenic Acid in a Neutral Phosphate Buffered Aqueous Solution from Femtoseconds to Final Products. *J. Phys. Chem. B* **2012**, *117*, 811–824.
- (59) http://en.wikipedia.org/wiki/Norrish_reaction.
- (60) Musa, K. A. K.; Eriksson, L. A. Photodegradation Mechanism of Nonsteroidal Anti-Inflammatory Drugs Containing Thiophene Moieties: Suprofen and Tiaprofenic Acid. *J. Phys. Chem. B* **2009**, *113*, 11306–11313.
- (61) Musa, K. A. K.; Eriksson, L. A. Photodegradation Mechanism of the Common Non-Steroid Anti-Inflammatory Drug Diclofenac and Its Carbazole Photoproduct. *Phys. Chem. Chem. Phys.* **2009**, *11*, 4601–4610.
- (62) Musa, K. A. K.; Eriksson, L. A. Theoretical Assessment of Norfloxacin Redox and Photochemistry. *J. Phys. Chem. A* **2009**, *113*, 10803–10810.
- (63) Musa, K. A. K.; Matxain, J. M.; Eriksson, L. A. Mechanism of Photoinduced Decomposition of Ketoprofen. *J. Med. Chem.* **2007**, *50*, 1735–1743.
- (64) Musa, K. A. K.; Eriksson, L. A. Theoretical Study of Ibuprofen Phototoxicity. *J. Phys. Chem. B* **2007**, *111*, 13345–13352.
- (65) Maillard, B.; Ingold, K.; Scaiano, J. Rate Constants for the Reactions of Free Radicals with Oxygen in Solution. *J. Am. Chem. Soc.* **1983**, *105*, 5095–5099.
- (66) Xu, M. S.; Wan, P. Efficient Photodecarboxylation of Aryl-Substituted Phenylacetic Acids in Aqueous Solution: A General Photochemical Reaction. *Chem. Commun.* **2000**, *21*, 2147–2148.
- (67) Ding, L.; Chen, X. B.; Fang, W. H. Ultrafast Asynchronous Concerted Excited-State Intramolecular Proton Transfer and Photodecarboxylation of O-Acetylphenylacetic Acid Explored by Combined Caspt2 and Casscf Studies. *Org. Lett.* **2009**, *11*, 1495–1498.
- (68) Graige, M. S.; Paddock, M. L.; Bruce, J. M.; Feher, G.; Okamura, M. Y. Mechanism of Proton-Coupled Electron Transfer for Quinone (Q_b) Reduction in Reaction Centers of Rb. Sphaerooides. *J. Am. Chem. Soc.* **1996**, *118*, 9005–9016.
- (69) Soudackov, A.; Hammes-Schiffer, S. Theoretical Study of Photoinduced Proton-Coupled Electron Transfer through Asymmetric Salt Bridges. *J. Am. Chem. Soc.* **1999**, *121*, 10598–10607.
- (70) Hammes-Schiffer, S. Theoretical Perspectives on Proton-Coupled Electron Transfer Reactions. *Acc. Chem. Res.* **2001**, *34*, 273–281.
- (71) Concepcion, J. J.; Brenneman, M. K.; Deyton, J. R.; Lebedeva, N. V.; Forbes, M. D. E.; Papanikolas, J. M.; Meyer, T. J. Excited-State Quenching by Proton-Coupled Electron Transfer. *J. Am. Chem. Soc.* **2007**, *129*, 6968–6969.
- (72) Hammes-Schiffer, S. Theory of Proton-Coupled Electron Transfer in Energy Conversion Processes. *Acc. Chem. Res.* **2009**, *42*, 1881–1889.
- (73) Hsieh, C.-C.; Jiang, C.-M.; Chou, P.-T. Recent Experimental Advances on Excited-State Intramolecular Proton Coupled Electron Transfer Reaction. *Acc. Chem. Res.* **2010**, *43*, 1364–1374.
- (74) Kaila, V. R. I.; Hummer, G. Energetics of Direct and Water-Mediated Proton-Coupled Electron Transfer. *J. Am. Chem. Soc.* **2011**, *133*, 19040–19043.